The International Journal of Advanced Manufacturing Technology
https://doi.org/10.1007/s00170-025-15654-0

ORIGINAL ARTICLE

A feasibility study on the circular manufacturing of sustainable metal additive manufacturing powders from machining chips

Debajyoti Bhaduri[1] · Karan A. Baramate[1] · Soumya Gangopadhyay[2] · Sukhwinder Singh[1] · Franck Lacan[1] · Michael Ryan[1]

Received: 31 January 2025 / Accepted: 27 April 2025
© The Author(s) 2025

Abstract

The holistic vision of the research is to develop a circular hybrid manufacturing framework to achieve 'Net Zero' for additive manufacturing sector by producing sustainable powders from production scrap/machining chips. This paper reports an initial feasibility study results from the foundation stage of the circular hybrid manufacturing framework that centres on generating additive manufacturing powders via solid-state crushing/ball milling of machining chips at room temperature. Here, the viability of the ball milling process to produce additive powders from three readily available chip materials is evaluated, viz. a low carbon steel (AISI 1020), and two aluminium alloy chips (AA6082-T6 and AA5083-H111). The ball-milled powders were characterised in terms of their morphology, size distribution, flowability and phase analysis. The morphology/size distributions were found to be influenced by the chip materials and their length scale. Single-track laser melting of pre-placed AA6082 ball-milled powder particles was subsequently performed to emulate the laser powder bed fusion process. Cross-sectional micrographs demonstrated melting and bonding of the ball-milled particles to the AA6082 substrate. A further feasibility trial was undertaken to fabricate cubes from the ball-milled AA5083 powders via the powder bed fusion process. The microhardness (71–88 $HV_{0.01}$) and microstructure of the specimens were comparable to rolled AA5083-H111 plates.

Highlights

- Foundation stage of a novel circular hybrid manufacturing (CHM) framework.
- CHM combines circular economy and hybrid manufacturing processes.
- Producing AM powders from machining chips via ball milling at room temperature.
- Fabricating simple LPBF cube structures from the ball-milled aluminium powders.
- Microhardness and microstructural analysis of the ball-milled LPBF parts.

✉ Debajyoti Bhaduri
BhaduriD@cardiff.ac.uk; debajyoti.bhaduri@gmail.com

[1] High-Value Manufacturing Research Group, School of Engineering, Cardiff University, Queen's Buildings, The Parade, Cardiff CF24 3AA, UK

[2] Department of Mechanical Engineering, Indian Institute of Technology Bhilai, Durg, Chhattisgarh 491002, India

Published online: 06 May 2025

Graphical Abstract

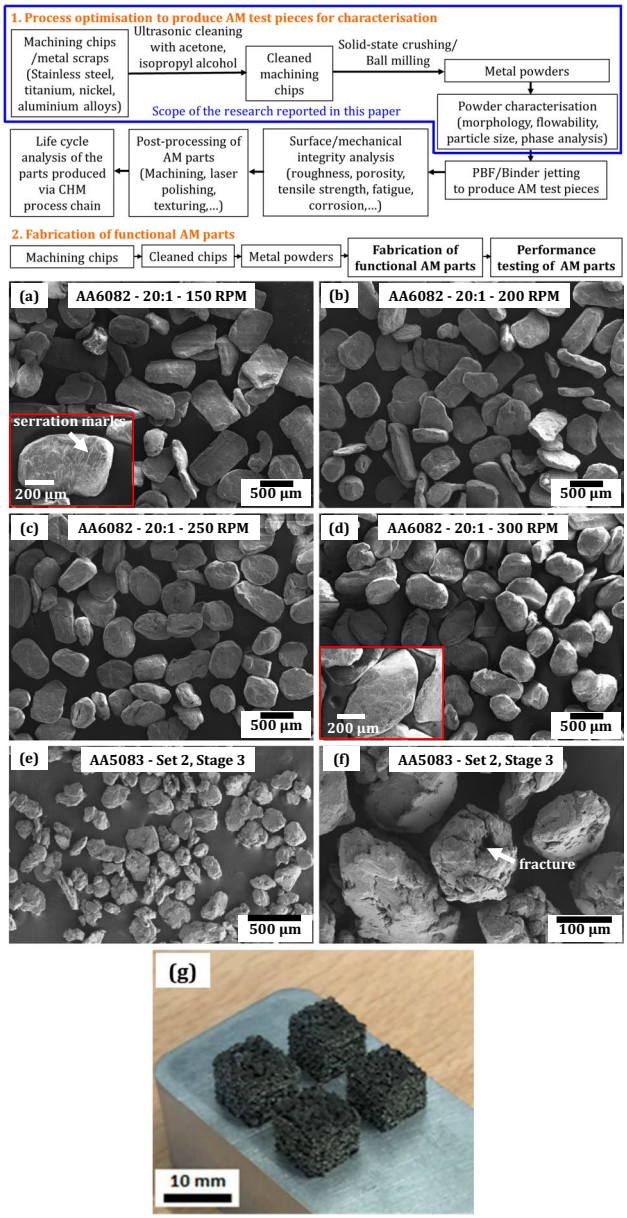

Keywords Additive manufacturing · Laser powder bed fusion · Circular economy · Ball milling · Machining chips · Aluminium

1 Introduction

Sustainable manufacturing is gaining momentum to meet United Nation's Sustainable Development Goals by minimising the environmental footprint of manufacturing processes. To achieve 'Net Zero' emissions by 2050, circular economy models in manufacturing, in contrast to the conventional linear economy, are increasingly being adopted via material recycling, reduction of energy consumption and energy recovery [1]. For additive manufacturing (AM), despite the immense benefits offered by the technology in terms of design freedom and material waste reduction [2], conventional AM powder production routes involving melting and atomisation processes (such as gas, water and plasma atomisation) consume substantial energy and have high carbon footprints. For example, 16–84 kg of CO_2 is released per kg of AM stainless steel powder production [3]. To mitigate this, reuse of commercial powders [4] as

well as alternative powder generation routes via solid-state crushing/ball milling (BM) of machining chips have been sporadically explored, although the majority of published work relating to the latter topic is aimed at powder metallurgy (PM) applications [5–8]. Shial et al. [5] and Teja et al. [6] explored the possibility of recycling titanium (Ti) chips, mixed with graphite (C) powders when ball milling. The produced in-situ Ti-TiC composite powders were utilised for fabricating pellets via sintering and compaction technique. Pulido-Suárez et al. [7] and Bhatta et al. [8] studied the use of ball-milled/crushed Al-Si-Zn-Mg and 4Cr5MoSiV chip powders to build discs via consolidation and sintering processes.

The use of BM powders for AM applications is a relatively new approach for materials' recycling. Thus far, BM powders in AM have been mainly tested when single-track melting operation, for example, laser-engineered net shaping of SS304L [9] and direct metal laser sintering of pre-placed Ti-6Al-4V powders [10]. In both cases, BM particles with irregular shape were obtained. Nonetheless, successful deposition of single tracks was accomplished. Fabrication of bulk test specimens using powder bed fusion (PBF) and directed energy deposition (DED) from BM heat-resistant steel chips is reported in a study by Razumov et al. [11]. This process, however, involved a secondary plasma spheroidisation step to impart greater particle sphericity, which would have increased the total energy consumption. Murray et al. [12] utilised direct feeding of cleaned and uncleaned machining chips into a DED machine to produce single-tracks. The deposition strategy involved both pre-placed and vibration-fed chips. A similar approach was explored by Dhami et al. [13] when using heated grinding swarf (sieved below 105 µm) to deposit single-tracks via DED process. Jackson et al. [14] demonstrated the possibility of fabricating DED tensile bars from irregular shaped BM 316L powder particles. The resulting tensile specimens showed marginally higher hardness, Young's modulus, ultimate tensile strength and yield strength, but lower elongation at fracture, compared to that produced from spherical gas-atomised powders. Wolff et al. [15] investigated in situ monitoring of the flow characteristic of plasma-atomised and ball-milled Ti-6Al-4V powders. They observed that while the plasma-atomised powder particles exhibited a laminar flow during deposition, the ball-milled swarf powder had a turbulent flow behaviour. Plasma-atomised powder caused steady melt pool dynamics and acicular microstructure, whereas the ball-milled swarf powder resulted in melt pool fluctuation and equiaxed microstructure.

Thus far, mechanically generated feedstock has mainly been used in DED processes. Further, the papers dealing with ball milling of machining chips have reported substantially long BM time, such as 2.5–12 h in [5, 6], 45–94 h in [7], 24–60 h in [9] and 6–18 h in [10]. Long BM time would expectedly increase the total energy consumption during the powder generation process, thus would impair the ultimate goal of the alternative mechanical route of AM powder production, i.e. reduction of energy consumption and CO_2 footprint.

The recently tested materials for generating BM powders from scrap are Ti-TiC [5, 6], Al-Si-Zn-Mg alloy [7], pure aluminium [16] and an alloy with 77% nickel content [17]. Examples of BM powder materials especially for AM applications include Fe-11%Cr-based steel [11], SS304L [9, 12], SS316L [14], AISI 52100 [13] and Ti-6Al-4V alloy [10, 15].

The holistic vision of the current research centres on the circular economy approach to produce sustainable metal AM powders by recycling production scrap and to provide solutions to 'zero waste' of materials. In particular, the research aims at developing a circular hybrid manufacturing (CHM) framework to generate AM powders via ball milling of machining chips, to fabricate and post-process AM components. The 'circular' aspect of CHM deals with recycling of materials. Here, the AM stage acts as a 'sink' for production scrap. The 'hybrid' term denotes that the framework involves both additive and subtractive (post-processing) stages. The holistic CHM concept is presented in Fig. 1a. The research reported in this paper focuses on the foundation stage of the CHM process chain, as shown in Fig. 1b. This includes assessing the viability of the BM process to produce metal AM powders, especially within shorter BM time as compared to that reported in the literature. Experimental trials were undertaken to produce and evaluate the BM powder characteristics, generated in-house from three readily available chip materials, viz. AISI 1020 carbon steel, and AA6082-T6 and AA5083-H111 aluminium alloys. These materials were chosen for their lower costs, compared to that of Ni or Ti-alloys. The steel chips were initially used to assess the suitability of the BM process for powder generation, as a proof-of-concept, whereas the Al-alloys were chosen for lightweight applications in the aerospace, automotive and marine sectors. To emulate the Laser-PBF (LPBF) AM process, single-track laser melting of the BM AA6082 powder was carried out. This was followed by a feasibility trial involving fabrication of LPBF cubes from BM AA5083 powder.

2 Material and methods

2.1 Ball milling

The Phase 1 proof-of-concept involved ball milling of AISI 1020 carbon steel chips (length scale ~ 1–3 mm), collected from conventional machining process. Machining was carried out on a Bridgeport Interact 2 vertical milling centre using 3-flute 20-mm milling cutters and using standard wet

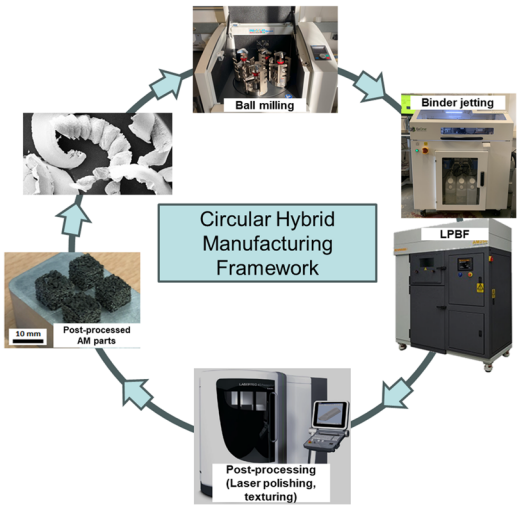

(a)

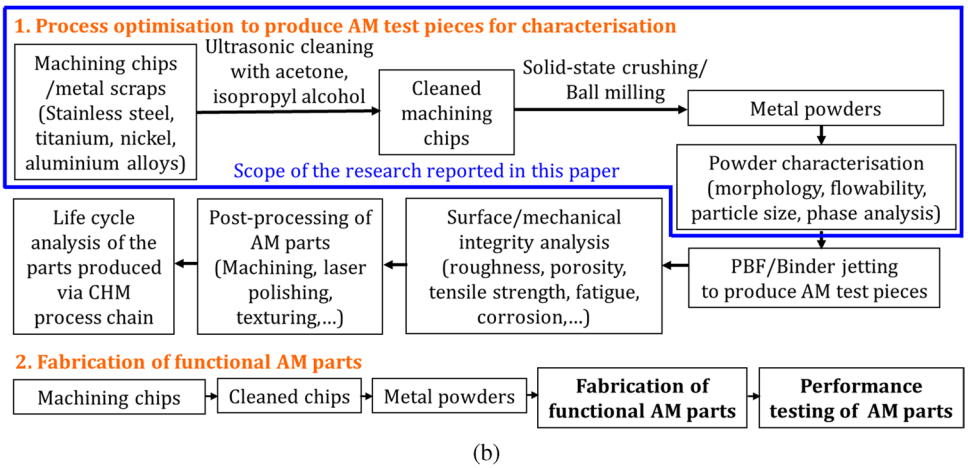

(b)

Fig. 1 **a** The holistic CHM framework to produce sustainable AM powders and fabricate functional AM parts. **b** The scope of the present paper is highlighted within the CHM process chain

end milling parameters (88 m/min cutting velocity, 0.3 mm/rev feed rate and 0.2-mm axial depth of cut). The chips were ultrasonically cleaned using acetone and isopropyl alcohol for 10 min for each cycle, followed by drying in an oven at 100 °C for 2 h. Based on the collective literature review [5, 6, 9, 10, 14], BM was carried out under dry atmospheric conditions on a Pulverisette 5/4 planetary ball mill, using 300 RPM, two 80 mL grinding jars and 29 off 10 mm balls in each jar, both made of hardened stainless steel. Three ball-to-powder ratios (BPR), 10:1, 30:1 and 50:1, were used for a BM time of 5 h, with a 10 min interval after each 10 min BM cycle (total processing time 9.83 h). A 4th trial using 50:1 BPR for 7 h was conducted to assess the effects of the BM time on the particle size, compared to the 3rd trial. The details of the BM parameters for the AISI 1020 steel chips are shown in Table 1. As Phase 1 was only to check the viability of ball milling to crush machining chips into particles and because carbon steel is typically not used in LPBF, no further powder characterisation (apart from particle morphology) or single-track melt test was carried out using carbon steel chip powder.

Table 1 Ball milling parameters used for AISI 1020 steel chips in Phase 1

	Ball-to-powder ratio (BPR)	Ball milling time (h)	BM RPM	Ball diameter (mm)
Trial 1	10:1	5	300	10
Trial 2	30:1	5		
Trial 3	50:1	5		
Trial 4	50:1	7		

Phase 2 experiments dealt with ball milling of two readily available aluminium alloy chips, AA6082-T6 (Phase 2A and 2B) and AA5083-H111 (Phase 3). Generation and cleaning of the aluminium chips were carried out in the same manner as in Phase 1. Here, Phase 2A was aimed at assessing the effects of varying BPR and BM time on the particle size and morphology. Thus, ball milling on the cleaned AA6082-T6

Table 2 Ball milling parameters used for AA6082-T6 aluminium chips in Phase 2

	Ball-to-powder ratio (BPR)	Ball milling time (h)	BM RPM	Ball diameter (mm)
Phase 2A	10:1	0.5	300	10
	20:1	3		
	30:1			
Phase 2B	20:1	0.5	150	10
			200	
			250	
			300	

milling chips was conducted at 300 RPM using the same jars and balls, with three BPRs (10:1, 20:1 and 30:1) and two BM durations (0.5 and 3 h). Substantial reduction in the BM time was chosen to save the total energy consumption, compared to the long milling hours typically used in [7, 9, 10]. Following this, Phase 2B trials explored the effects of the ball milling rotational speed (RPM) of the grinding jars. Thus, the trials involved variation in the BM RPM (150, 200, 250 and 300) with a fixed BPR (20:1) and BM time (0.5 h), as shown in Table 2.

To assess the scope of the BM process on a different larger ball miller, with multi-stage operation as well as for a diverse range of materials Phase 3 experiments involved dry BM of cleaned AA5083-H111 chips on a Mechmin planetary ball mill. Following comprehensive initial trials involving multiple combinations of varied BPR (10:1, 15:1, 20:1 and 30:1), ball diameter (5, 10, 20 mm), BM time (0.5, 1, 1.5 h), RPM (150, 300, 500) and jar volume (100 and 250 mL), the finally selected multi-stage BM settings are shown in Table 3. After stage 1, powders with < 180 µm size were sieved and used for the subsequent stages.

The nominal compositions of all the three tested materials, together with their indicative hardness values are presented in Table 4 [18].

2.2 Powder characterisations

The maximum impact force (F) per collision during the planetary BM was estimated using the Eq. (1) used in [9, 19].

$$F(t) = ma(t) = m\left\{4\pi^2\omega^2\left[R^2plate + R^2jar + 2R_{plate}R_{jar}cos(4\pi\omega t)\right]^{1/2}\right\} \quad (1)$$

where where m is the mass of the ball, a is the acceleration rate, t is time, ω is the angular speed of rotation, R_{Plate} is the radius of the main disc and R_{Jar} is the internal radius of the jar.

The powder morphology, composition and electron back scattered diffraction (EBSD) analysis were conducted using Carl Zeiss and Tescan Maia FEG scanning electron microscopes. Particle size analysis of the AISI 1020 was carried out via laser granulometry using a Malvern Mastersizer 3000 system. Due to a comparatively larger particle size of the Al powders laser granulometry deemed unsuitable. Thus, sieving technique was used to classify the AA6082 and AA5083 powders in different size classes.

Table 3 Two sets of multi-stage BM parameters used for AA5083-H111 aluminium chips in Phase 3

BM sets		BPR	Ball diameter (mm)	Jar vol. (mL)	BM RPM	BM time (h)
Set 1	Stage1	15:1	20	250	300	1
	Stage 2	10:1	10	250	300	0.5
	Stage 3	10:1	5	100	150	1
Set 2	Stage 1	15:1	20	250	300	1
	Stage 2	10:1	10	250	500	0.5
	Stage 3	10:1	5	100	150	1

Table 4 Elemental weight percentage and indicative hardness of (a) AISI 1020, (b) AA6082-T6 and (c) AA5083-H111 materials

(a)								
Material	Hardness	C	Mn	P	S	Fe		
AISI 1020	126 HV	0.17–0.23	0.30–0.60	≤ 0.040	≤ 0.050	Bal.		
(b)								
Material	Hardness	Si	Mg	Mn	Cr	Cu	Fe	Al
AA6082-T6	95 HV	0.7–1.3	0.6–1.2	0.4–1.0	≤ 0.25	≤ 0.1	≤ 0.5	Bal.
(c)								
Material	Hardness	Si	Mg	Mn	Cr	Cu	Fe	Al
AA5083-H111	75 HV	0.4	4.0–4.9	0.4–1.0	≤ 0.25	≤ 0.1	≤ 0.4	Bal.

Following this, phase detection was carried out using a Siemens D5000 X-ray diffractometer with a Cu-Kα target, 0.02° step size, 1.2 s/step scan speed, 40 kV voltage and 30 mA current, within a 2θ range of 30°–85°. Powder flowability was analysed using a Hall Flowmeter (Qualtech Products Ltd, UK), according to ASTM B213-17 [20].

2.3 Single-track melting of BM powder and fabrication of LPBF cubes

Since the Phase 1 ball milling of AISI 1020 steel chips were carried out as a proof-of-concept only, no further experiments were conducted to build AM test parts using the BM steel powder. In contrast, to emulate the use of ball-milled aluminium powders in AM, single-track laser melting of pre-placed AA6082 BM particles, produced with 20:1 BPR for 0.5 h at 300 RPM and sieved to < 425 µm, was carried out on an AA6082 substrate in a Renishaw AM250 pulsed LPBF system. The particle size range was greater than that typically used for LPBF; however, single-track melt tests were carried out to inspect the melting and bonding ability of the particles with the substrate. Five tracks were produced in an argon environment using a 200 W pulsed fibre laser with a 60 µm spot size. Due to the large particle size, powder particles on each track (T) were melted using two successive sets of laser energy densities (E_d, J/mm^3), viz. T1: 120, 480; T2: 227, 603; T3: 243, 724; T4: 305, 843 and T5: 362, 962.

Similarly, single track melting of BM AA5083 powder particles via LPBF has also been conducted and the results have been reported elsewhere [21].

The viability of the BM powders to fabricate simple structures were further assessed by building four LPBF cubes (8 × 8 × 10 mm L × W × H) using the ball milled AA5083 powder particles. This time, lower particle size was used that were sieved to < 180 µm. Four different laser energy densities (28, 55, 82 and 133 J/mm^3) were employed to fabricate the four specimens. A 200 W laser power, 0.18 mm layer thickness, 0.13 mm hatch spacing and 67° rotation between adjacent layers were utilised, together with varying exposure time to achieve the four energy density levels. These parameters for AA5083 alloy powder were chosen according to [22].

Cross-sectional microhardness and microstructure evaluation of the AA6082 single-track particles and AA5083 LPBF cubes were subsequently evaluated. Microhardness measurements were carried out using 10 g load and 10 s dwell time. Microstructures were revealed via immersion etching with Keller's reagent (2 mL hydrofluoric acid, 3 mL hydrochloric acid, 5 mL nitric acid and 190 mL deionised water) for 1 min.

3 Results and discussion

3.1 Powder morphology and particle size distribution analysis

The SEM images of the AISI 1020 steel chips and the ball miller powders produced from the chips at varying BPR and BM time are shown in Fig. 2. The length scale of the steel chips was at the order of ~ 1–3 mm (Fig. 2a). This was much larger compared to the mean chip size (~ 120–420 µm) of medium carbon steel (0.48% C) chips used for building thin wall structures via laser metal deposition by Mahmood et al. [23]. The ball milled AISI 1020 steel powders were mostly flaky and irregular shaped as shown in Fig. 2b–e, although the particle size visibly reduced with the increase of BPR.

The SEM micrographs of the AA6082 aluminium chips and the corresponding BM powders are displayed in Fig. 3. The length scale of the AA6082 chips was comparable with that of the steel chips (~ 1–3 mm), as seen from Fig. 3a). However, the BM AA6082 powder particles had relatively greater sphericity, albeit with a much larger average particle size than that of the steel powder (Fig. 3b–d).

Laser granulometry (Fig. 4a) revealed that average particle size of the AISI 1020 steel powder decreased with increasing BPR from 10:1 to 50:1, due to the greater crushing effect by the balls at higher BPR. While 90% (by volume) of the analysed particles had < 60 µm average size when using 10:1 BPR, the equivalent volume had < 26 µm average size when BM with 50:1 BPR. Average steel particle size slightly increased (~ 35 µm) when milled for longer hours (7 h), possibly due to powder agglomeration/cold-welding [9]. The cold-welding effect was more prominent on the AA6082 powder as the material has comparatively lower hardness (95 HV) and ultimate tensile strength (290 MPa) than AISI 1020 (~ 126 HV and ~ 426 MPa, respectively) [24]. With 3 h BM time and 10:1 BPR, the accumulated impact force was not sufficiently high to reduce the aluminium particle size, only 14% (by weight) of the produced powders were < 600 µm. Greater powder quantity with < 600 µm size was obtained (~ 75%) with the 20:1 BPR, however with increased BPR (30:1) the average particle size increased again owing to cold-welding (Fig. 4b). With the shorter BM time (0.5 h), ~ 56–64% of the powders were < 600 µm for the tested range of BPR (Fig. 4b).

Since 20:1 BPR and 0.5 h BM time setting gave more than 60% particles below 425 µm average size within a short BM time, these settings were selected for the subsequent Phase 2B trials, while the jar RPM was varied. It was observed that the distributions of the particle size

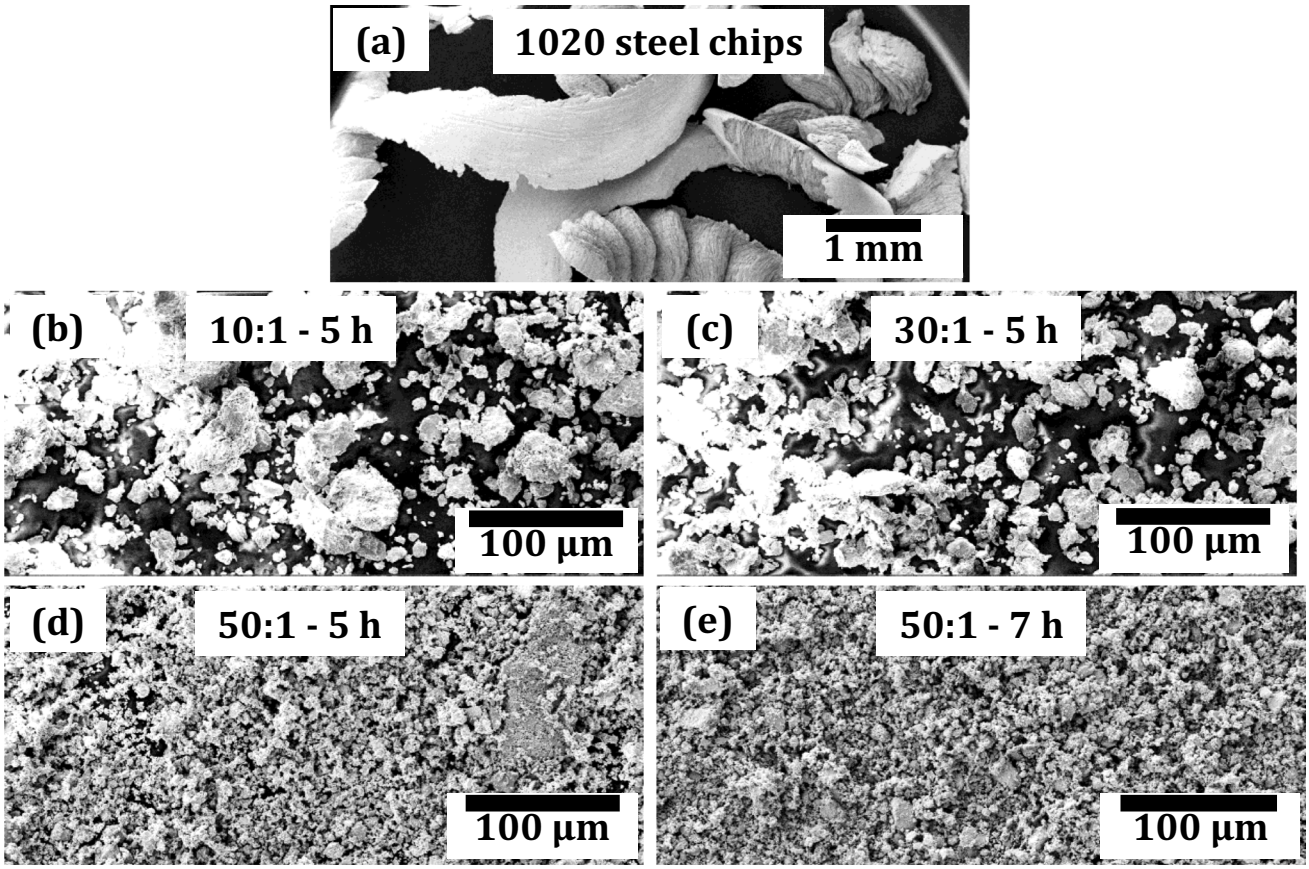

Fig. 2 SEM images of **a** AISI 1020 chips, and BM steel powders obtained with BPRs of **b** 10:1, **c** 30:1, **d** 50:1 after 5 h and **e** BPR of 50:1 after 7 h in Phase 1

classes were comparable for all four ball milling speeds (RPM), with ~ 67–78% of the BM particles had < 600 µm average size, as seen from Fig. 4c. However, the SEM images in Fig. 5a and b revealed flattened particles with larger aspect ratio following BM with lower speeds (150–200 RPM), whereas higher speeds (250 and 300 RPM) resulted in greater sphericity (Fig. 5c and d). The inset image in Fig. 5a shows remains of the chip serration marks; thus, the chips did not fully convert to powders when using lower RPM. This was because of the lower impact force exerted at lower levels of RPM, for example, 0.06 N impact force was generated per collision at 150 RPM. In contrast, BM with higher RPM (such as 300) would exert 0.44 N force per collision, resulting in greater plastic deformation of the chips, leading to enhanced particle sphericity. Thus, Phase 2 established that a higher BM RPM is required to break down chips into particles.

Based on the observations from Phase 2 trials, Phase 3 BM was conducted in multiple stages, as recommended in [9], with larger balls (20 and 10 mm diameter balls) and higher RPM (300 and 500) to first breakdown the chips into smaller particles. Following this, smaller balls (5 mm diameter) and lower RPM (150) were used to refine the particle morphology. Using this strategy, ~ 30–40% (by weight) of the total generated powders after Stage 1 BM had < 180 µm average size which were further sieved to obtain the particle size class distributions, as shown in Fig. 4d. Following Set 2-Stage 3 BM, ~ 70% of the powder particles were < 150 µm. The powder morphology (Fig. 5e and f) reveals a mixture of plastic deformation and cleaved fracture. Since the AA5083 alloy has higher Mg content (4–4.9%) compared to that in AA6082 alloy (0.6–1.2%) [24], the greater strain-hardening ability of the former alloy under the action of higher impact forces, (3.8 N/collision with 20 mm balls as determined using Eq. 1), during BM caused crack propagation within the particles, leading to brittle fracture. This could be attributed to the greater percentage of powder particles of less than 150 µm size obtained from the AA5083 chips, compared to that produced from the AA6082 chips.

3.2 Powder flowability analysis

The flowability analysis of the AISI 1020 powder showed irregular flow because of the cohesive nature of the flaky

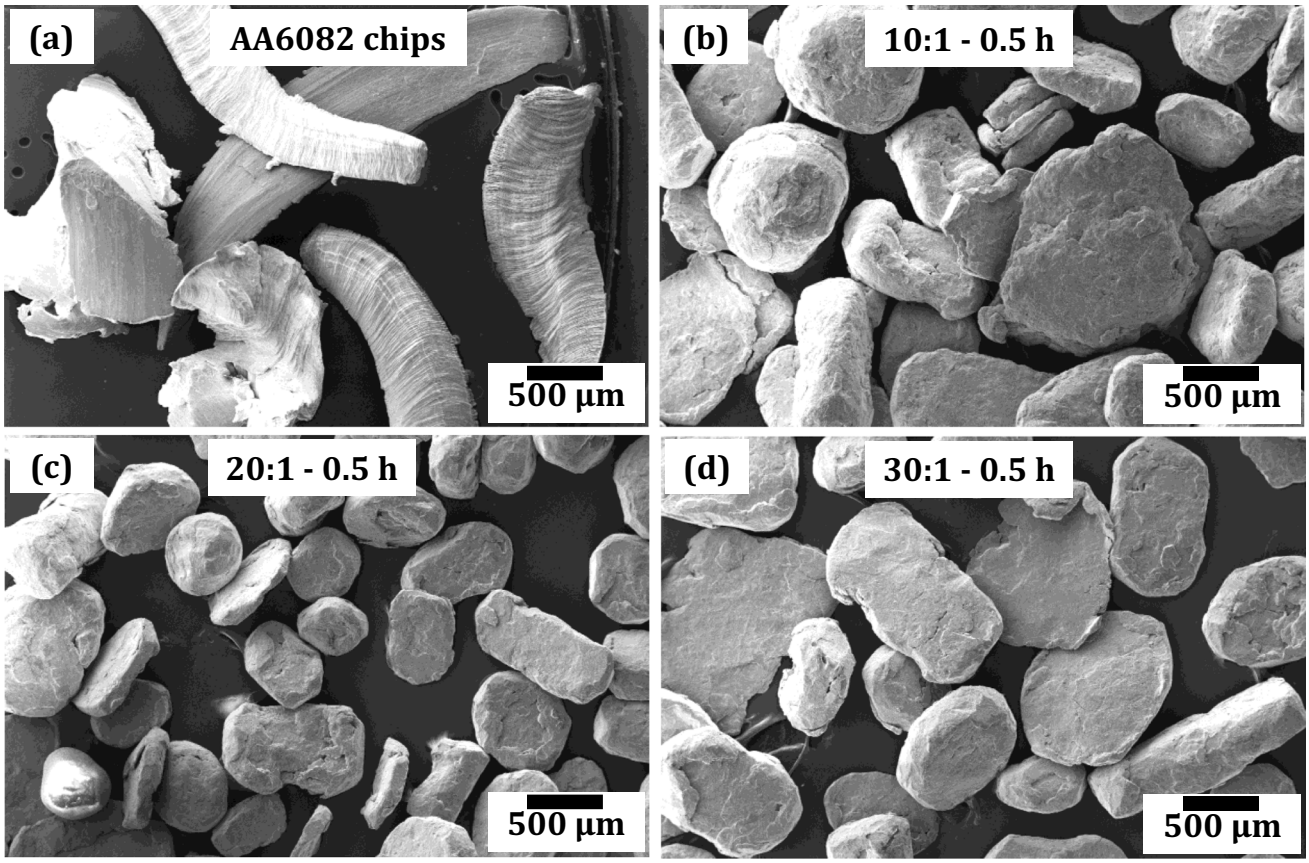

Fig. 3 SEM images of **a** AA6082 chips, and BM AA6082 powders collected with BPRs of **b** 10:1, **c** 20:1 and **d** 30:1 after 0.5 h in Phase 2A

steel particles. Conversely, the two aluminium powder materials exhibited smoother flow. The flow rates of 1.5 g of AA6082 powder (due to limited quantity produced) from each batch with < 425 µm size were recorded. The Phase 2A powders displayed varied flow rates between 1.35 and 2.44 s without any specific trend. In contrast, the flow rates of the Phase 2B powders decreased from 3.2 to 1.94 s with increasing BM speed from 150 to 300 RPM. The elongated/partially converted powders obtained with lower RPM (evident from Fig. 5 a and b) attributed to their lower flow rates.

The flow rates of 25 g of Set 1 and Set 2 AA5083 powders (< 180 µm) were tested (due to limited quantity) and compared with the equivalent weight of commercial gas atomised AlSi10Mg (~ 30–60 µm) powder. A further flowability comparison between 50 g of the latter two powder specimens was undertaken to comply with the ASTM B213-17 Standard. The repose angles measured from the flowability test using Hall Flowmeter on 25 g of AA5083 and AlSi10Mg powder specimens are shown in Fig. 6. The flow rate of the Set 2 AA5083 powder was slightly higher (31.22 s/25 g) than that of the Set 1 powder (33.52 s/25 g), together with a lower angle of repose (AOR = 32.5°) of the Set 2 sample (Fig. 6), possibly because of the greater percentage of < 150 µm particles in Set 2 (evident from Fig. 4d). Although a comparison between the flow rates of the BM powders and that of the commercial AlSi10Mg was not a true like-for-like scenario, this was carried out since AlSi10Mg is a readily available off-the-shelf candidate for LPBF processes. Despite the marginally lower flow rate (36.49 s/25 g), a 15% lower AOR was measured on the AlSi10Mg, compared to the Set 2 BM powders. This could be due to a combination of the cohesiveness and sphericity of the AlSi10Mg particles, having a size range of ~ 30–60 µm. A similar trend was observed when 50 g of the Set 2 AA5083 and AlSi10Mg powders were tested. While the former specimen displayed a flow rate of 60.1 s/50 g and 35° AOR, the same for the latter were 77 s/50 g and 30°. Based on the AOR values, the tested AA5083 powders can be classified as 'free-flowing' [25].

3.3 Phase analysis

The phase analysis on the AA6082 and AA5083 milling chips and powders using XRD is presented in Fig. 7. The XRD spectra exhibited standard Al peaks at the 2θ positions, aligning with the JCPDS card 04–0787. Presence of aluminium oxide may also be possible as the

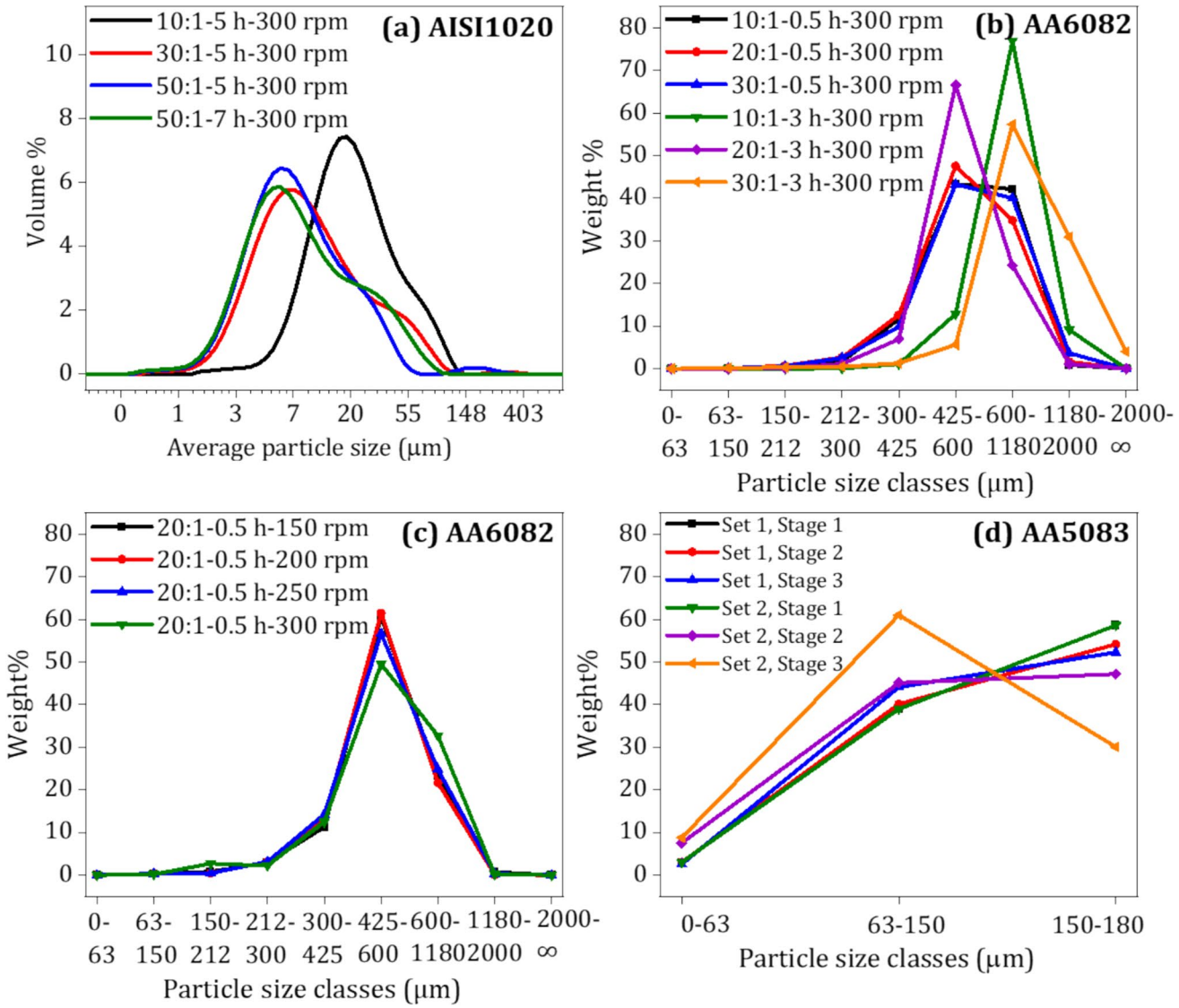

Fig. 4 Particle size analysis of **a** AISI 1020 in Phase 1, **b** AA6082 powder in Phase 2A and **c** in Phase 2B, **d** AA5083 powder in Phase 3

peak positions for Al_2O_3 at 38.2° and 77.8° are in agreement with JCPDS card 002–1227. This is supported by the detection of ~ 4.7–7.6 wt% oxygen in the Al powders via energy-dispersive spectroscopy (EDS). The formation of oxides is expected as the ball milling was carried out under dry atmospheric conditions. Nonetheless, the effects of the oxide formation on the AM parts' mechanical properties are within the scope of further research. In addition, the marginal left shifts of the powder specimens' peaks from that of the chips is an indication of compressive stresses within the particles, resulted from the mechanical impact forces during BM.

3.4 Single-track melting of BM powder and fabrication of LPBF cubes

Visual images of the single-tracks of pre-placed AA6082 powder particles (sieved under 425 μm size), melted via LPBF, are shown in Fig. 8a. Although a minor proportion of the particles was ~ 63–150 μm, the majority of the particles were much larger than that of standard commercial LPBF powders. Nonetheless, the trials were carried out to assess the feasibility of melting the BM powders using laser irradiation. The lowest laser energy density (E_d = 120 J/mm^3) on T1 was selected as per Renishaw's

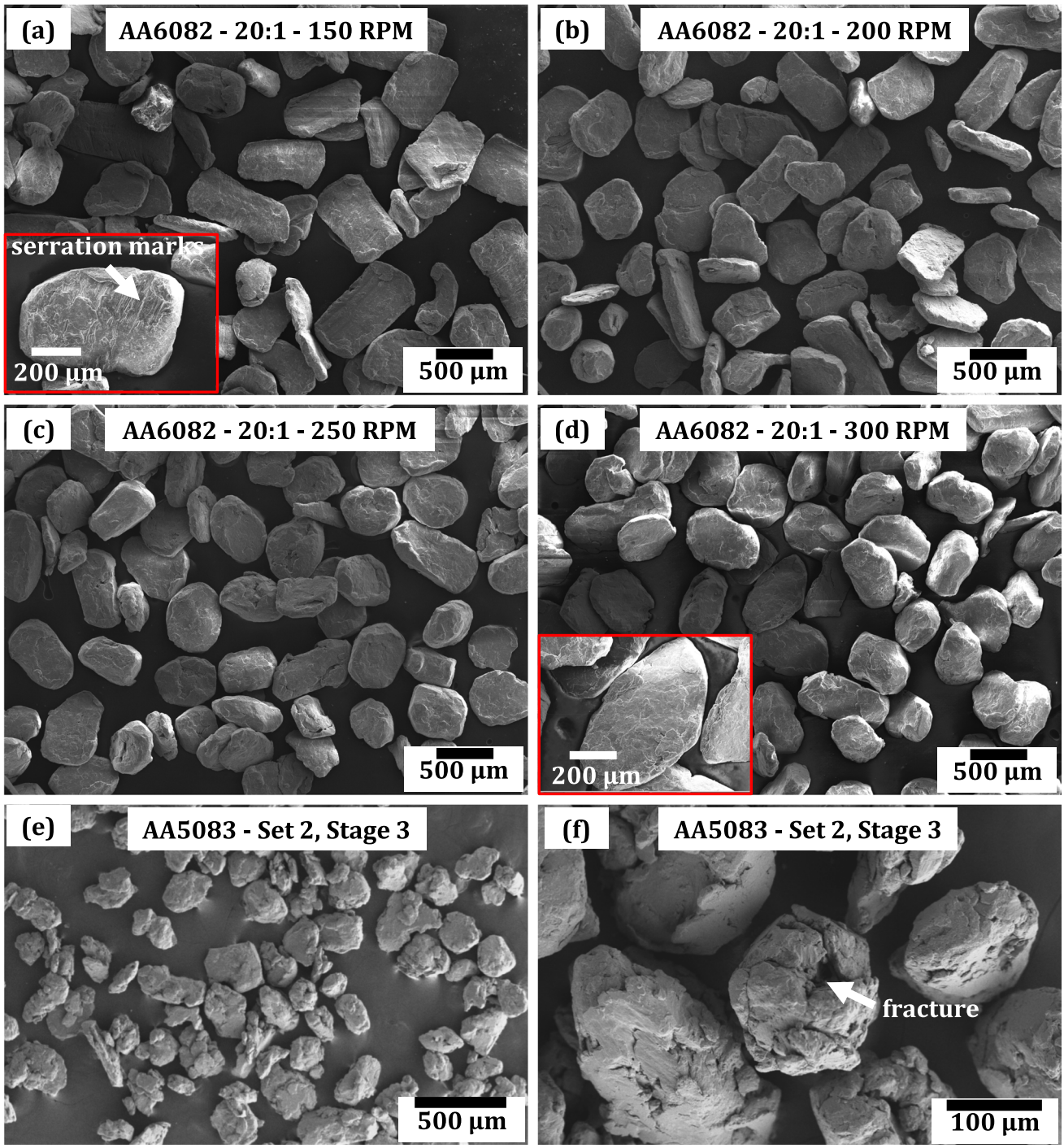

Fig. 5 SEM images of AA6082 powder in Phase 2B with **a** 150, **b** 200, **c** 250 and **d** 300 BM RPM; **e**, **f** SEM images of AA5083 powder after Set 2-Stage 3 in Phase 3

recommended settings for AlSi10Mg. However, the lower E_d values (120–362 J/mm^3) were not sufficient to bond the AA6082 particles to the AA6082 substrate. Thus, a subsequent series of laser irradiation was conducted on the same track positions using higher E_d values (480–962 J/mm^3). The evidence of successful melting and bonding of powder particles with the substrate can be seen in Fig. 8e while the laser irradiation marks on top of a melted particle from T5 are visible in Fig. 8b. The degree of melting expectedly increased with the rise in E_d, with ~ 115 µm melted depth, aligning with the Gaussian distribution of laser energy (Fig. 8c). However, few keyhole pores are

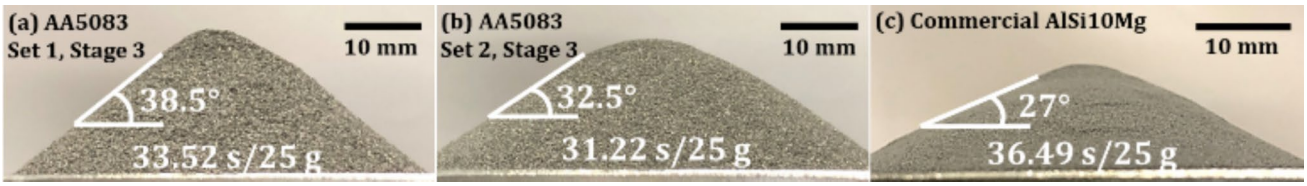

Fig. 6 Flowability test using Hall Flowmeter on 25 g of AA5083 and AlSi10Mg powder specimens, showing the angles of repose

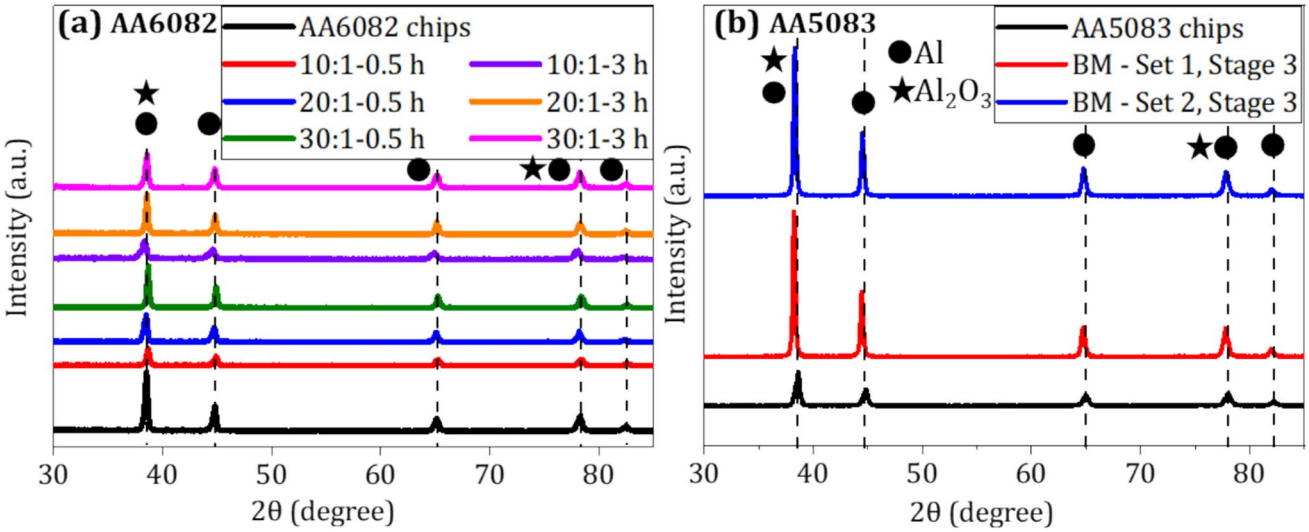

Fig. 7 **a** Phase analysis of AA6082 and **b** AA5083 chips and powders using XRD

also seen in Fig. 8d, suggesting that the E_d was possibly too high, causing the 'keyhole' effects.

The average microhardness of a bonded particle shown in Fig. 8c was noted as ~ 73 $HV_{0.01}$. This was ~ 16% lower than that of the bulk material (~ 87 $HV_{0.01}$), possibly due to the thermal softening of the powder material at high E_d. The microstructure of the particle in Fig. 8d exhibits orientation of the grains along the cooling direction near the bonding interface. This is supported by the EBSD inverse pole figure (shown in Fig. 8f) taken on the large, melted particle in Fig. 8c. The grains however have different texture orientations. Presence of Mg and Si phases as well as some oxide formations were detected within the Al matrix, as evident from the EDS spectra in Fig. 9 and through the elemental analysis presented in Table 5. Greater precipitation of Si upon laser irradiation is apparent, with a ~ 9.25 weight% within the matrix as compared to the nominal values (0.7–1.3%). Similar observation was reported when pulsed laser polishing of LPBF parts fabricated from a commercial AlSi10Mg alloy [26].

Since a large proportion of the BM AA6082 particles was typically in the range of 425–600 µm, these were not further tested for fabricating cubic structures using LPBF. On the other hand, BM AA5083 particles were tested for building cubes as the majority of the particles was below 180 µm.

Prior attempt of fabricating 3D structures using ball milled powder feedstocks involved DED AM process [14, 23]. Therefore, this study assessed the feasibility of building simple cubic structures using BM particles via LPBF process. The fabrication of four LPBF cubes from the ball milled AA5083 powder was carried out using a specially designed and built in-house reduced volume kit (RBV), shown in Fig. 10a. The bespoke RBV is capable of accommodating and printing when using a small volume of feedstock powder. Figure 10b and c display the LPBF fabrication process of the cubes from the BM AA5083 powder particles. The fabrication of the cubes in this study demonstrates that it is possible to build LPBF 3D structures from recycled production scrap that are crushed in solid-state at room temperature. Images of the four built cubes are shown in Fig. 10d.

It is worth noting that the ball milled powders used in this study for fabricating the LPBF structures were generated in a substantially shorter BM time, i.e. 2.5 h only, compared to the long BM time reported in the literature, e.g. 2.5–12 h in [5, 6], 45–94 h in [7], 24–60 h in [9] and 6–18 h in [10]. Unlike the study by Razumov et al. [11], no post-processing

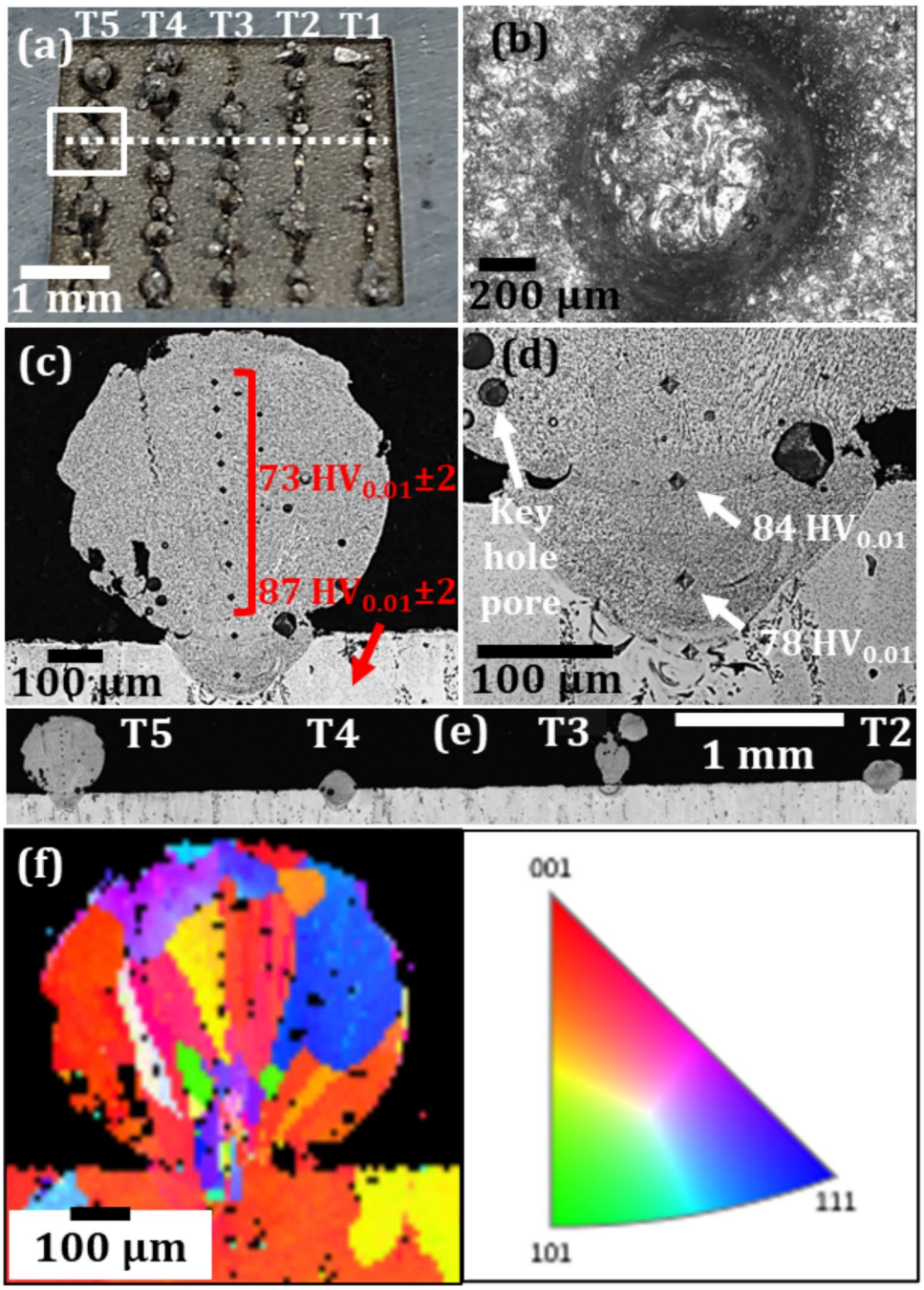

Fig. 8 **a** Five single-tracks of AA6082 powder particles (sieved to < 425 µm) melted via LPBF, **b** a molten particle on track T5, **c** cross-section of the particle showing the average hardness values and **d** microstructure, **e** molten AA6082 particles from T2 to T5, bonded with the substrate, **f** EBSD inverse pole figure taken on the particle in image **c.**

of the BM powders was carried out in the present research. However, the surface quality of the cubes was visually rougher. This was expected as larger particle size was used (sieved down to < 180 µm), whereas typical particle size range of the commercial AlSi10Mg powder for LPBF is between ~ 20 and 60 µm. A representative SEM image of a cube's top surface (Fig. 11a) exhibits melted and agglomerated particles, together with signs of laser track marks. A magnified image (Fig. 11b) shows the evidence of the flow of molten material under surface tension. The melted and solidified particles on the side walls (Fig. 11c) were visibly smaller than that on the top surface. These are believed to be partially melted particles on top of larger agglomerated particles underneath. The cross-sectional microstructure (Fig. 11d) shows the presence of large quantity of strengthening precipitates within Al matrix, with no clear signs of grain boundaries. The cross-sectional microhardness data is presented in Fig. 12. Despite the rougher appearance of the cubes, the microhardness values recorded along (71–81 $HV_{0.01}$) and transverse (76–88 $HV_{0.01}$) build directions were comparable to that of rolled AA5083-H111 plates (80 HV_1) [27]. This indicates that the inter-particle bonding

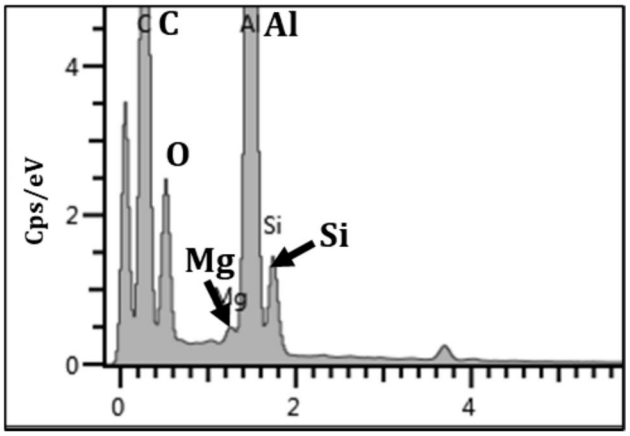

Fig. 9 Energy-dispersive spectroscopy (EDS) spectra obtained from the mapping of the particle in Fig. 8c

Table 5 EDS elemental analysis obtained from the mapping of the particle in Fig. 8c

Elements	Weight%
Al	73.04
Si	9.25
Mg	0.88
O	16.83
Total	100.00

has taken place to attain microhardness values similar to that of conventionally produced rolled plates. The hardness values were lower than as-built LPBF AlSi10Mg parts (~ 122–142 $HV_{0.01}$), reported in a previous study by the authors [28]. This is due to the greater Si content (9–10 weight%) in AlSi10Mg compared to AA5083 as shown in Table 4.

4 Conclusions

The research reported in this paper is foundational for the development of a novel circular hybrid manufacturing framework using recycled production scrap. This work demonstrates that machining chips of readily available materials can be converted into the powders suitable for metal AM, via ball milling process within a short BM time, such as 2.5 h only. The results indicate that, a higher ball milling speed (RPM) is required to crush machining chips into powder particles. It was further observed that the efficiency of the BM process as well as the morphology and particle size distribution of the powder particles are affected by the chip material. Carbon steel is harder than aluminium alloys, thus, breaking of steel chips into smaller particles was achievable. In contrast, plastic deformation and agglomeration of particles were typically observed on the softer AA6082 and AA5083 alloy powders. From the

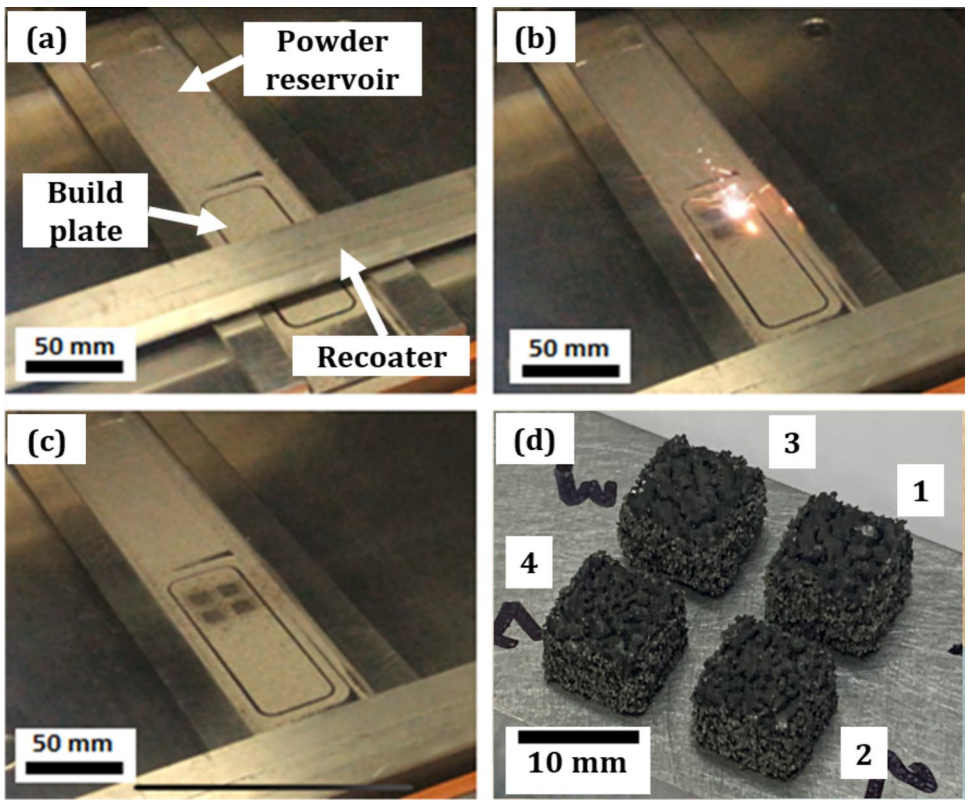

Fig. 10 **a** In-house manufactured reduced volume kit (RBV), **b** laser irradiation of AA5083 powder, **c** building process of the cubes, **d** fabricated LPBF AA5083 cubes

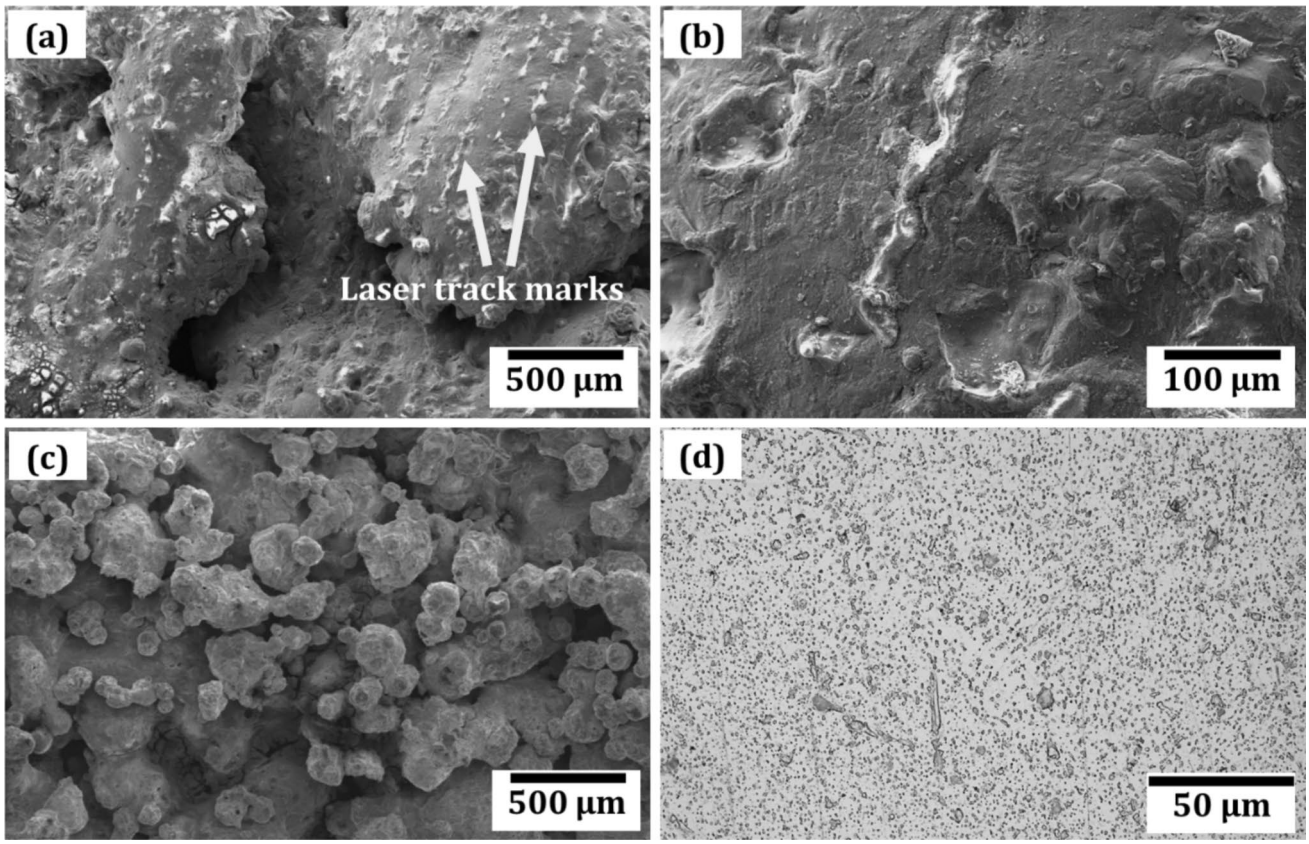

Fig. 11 a SEM images of the top face of an AA5083 cube, **b** magnified view, **c** SEM image of the side wall, **d** cross-sectional microstructure

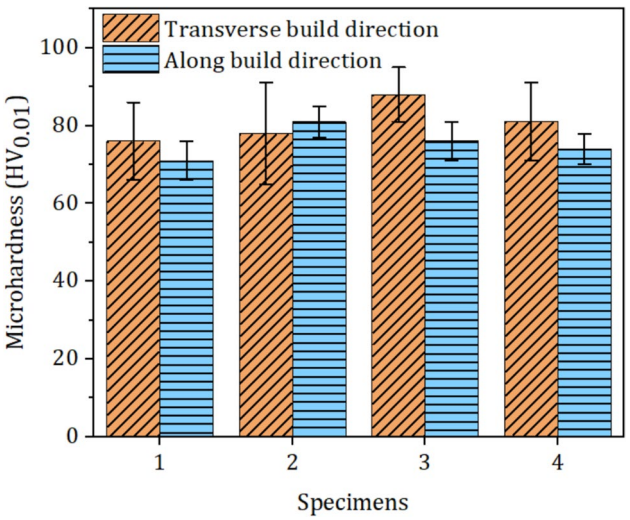

Fig. 12 Microhardness data measured on the cross-sections of the cubes along and transverse build directions (5 measurements taken for each dataset)

standpoint of solid-state crushing, materials with higher hardness and lower ductility would be more suitable for powder generation by fracture. Even though the produced powders were not typically spherical as compared to the gas-atomised powders, they can be used in PBF, DED and binder jetting processes as evidence of using irregular water atomised or ball milled powders in PBF is available [29]. This study utilised two grinding jars of different volumes, such as 80, 100 and 250 mL. Thus, the process can be scaled up by utilising larger jars, such as commercially available 500 mL jars, and by operating machines in parallel, to become scalable for industrial adoption.

The present research will continue evaluating the capability of the solid-state crushing/ball milling process for other materials, for example, Ti-6Al-4V. It is worth mentioning that in another study by the authors, Ti-6Al-4V machining chips of length scale up to ~30 mm have been successfully crushed to powder particles of < 100 µm size. Thus, it is evident that ball milling is capable of producing powders from longer chips. Rectangular test pieces have been printed and sintered from the ball milled Ti-6Al-4V powder particles via a metal binder jetting AM process. A comparative analysis of the surface and mechanical properties of the binder jetted parts made from ball milled chip powder and commercial gas atomised powder has been reported [30]. Subsequent research will involve assessing the effects of scrap source, compositions and cleaning procedures, together with the

oxide formation during BM (when conducted under dry atmospheric conditions) in relation to the parts' surface, mechanical and thermal properties.

Although a life-cycle analysis was not within the scope of this initial feasibility study, future work will also necessarily include the life-cycle analysis of the CHM framework for selected materials to estimate the total energy consumption and CO_2 footprint. The results will be compared with the available industrial data on metal AM processes using commercial powders.

Acknowledgements The authors further acknowledge the ERDF (European Regional Development Fund) and Wolfson Foundation for funding the CCI (Cardiff Catalysis Institute) Electron Microscopy Facility.

Author contribution Debajyoti Bhaduri: conceptualization; funding acquisition; project administration; supervision; writing—original draft.

Karan A. Baramate: investigation; data curation; formal analysis.

Soumya Gangopadhyay: conceptualization; funding acquisition; supervision; writing—review and editing.

Sukhwinder Singh: investigation; resources; data curation.

Franck Lacan: investigation; supervision; data curation.

Michael Ryan: supervision; writing—review and editing.

Funding The authors acknowledge the Welsh Government's Sêr Cymru Enhancing Competitiveness Equipment Fund, Cardiff University's Net Zero Innovation Institute Fund, the Government of Maharashtra's (India) PhD studentship award (Rajarshi Shahu Maharaj Foreign Scholarship) and the Indian Government's Scheme for Promotion of Academic and Research Collaboration (SPARC) grant (Project code: P2968).

Declarations

Conflict of interests The authors declare that they have no known competing financial interests or personal relationships that could have appeared to influence the work reported in this paper. The author is an Editorial Board Member/Editor-in-Chief/Associate Editor/Guest Editor for *[Journal name]* and was not involved in the editorial review or the decision to publish this article.

Open Access This article is licensed under a Creative Commons Attribution 4.0 International License, which permits use, sharing, adaptation, distribution and reproduction in any medium or format, as long as you give appropriate credit to the original author(s) and the source, provide a link to the Creative Commons licence, and indicate if changes were made. The images or other third party material in this article are included in the article's Creative Commons licence, unless indicated otherwise in a credit line to the material. If material is not included in the article's Creative Commons licence and your intended use is not permitted by statutory regulation or exceeds the permitted use, you will need to obtain permission directly from the copyright holder. To view a copy of this licence, visit http://creativecommons.org/licenses/by/4.0/.

References

1. Kara S, Hauschild M, Sutherland J, McAloone T (2022) Closed-loop systems to circular economy: a pathway to environmental sustainability? CIRP Ann Manuf Technol 71:505–528
2. Thompson KA, Moroni G, Vaneker T, Fadel G, Campbell RI, Gibson I, Bernard A, Schulz J, Graf P, Ahuja B, Martina F (2016) Design for additive manufacturing: trends, opportunities, considerations, and constraints. CIRP Ann Manuf Technol 65:737–760
3. Van Sice C, Faludi J (2021) Comparing environmental impacts of metal additive manufacturing to conventional manufacturing, International Conference on Engineering Design, ICED21, Gothenburg, Sweden, 671–680.
4. Terrassa KL, Haley JC, MacDonald BE, Schoenung JM (2018) Reuse of powder feedstock for directed energy deposition. Powder Technol 338:819–829
5. Shial SR, Masanta M, Chaira D (2018) Recycling of waste Ti machining chips by planetary milling: generation of Ti powder and development of in situ TiC reinforced Ti-TiC composite powder mixture. Powder Technol 329:232–240
6. Teja PJ, Shial SR, Chaira D, Masant M (2020) Development and characterization of Ti-TiC composites by powder metallurgy route using recycled machined Ti chips. Materials Today: Proceedings 26:3292–3296
7. Pulido-Suárez PA, Uñate-González KS, Tirado-González JG, Esguerra-Arce A, Esguerra-Arce J (2020) The evolution of the microstructure and properties of ageable Al-Si-Zn-Mg alloy during the recycling of milling chips through powder metallurgy. J Market Res 9(5):11769–11777
8. Bhatta G, De Los SV, Liu X, Ma Z, Bustamante Domínguez AG, Moreno NO, Espinoza Suarez SM, Barnes CHW, Zhang D (2021) Microstructure and mechanical properties of solid state recycled 4Cr5MoSiV (H11) steel prepared by powder metallurgy. Results in Materials 10:100184
9. Fullenwider B, Kiani P, Schoenung JM, Ma K (2019) Two-stage ball milling of recycled machining chips to create an alternative feedstock powder for metal additive manufacturing. Powder Technol 342:562–571
10. Dhiman S, Joshi RS, Singh S, Gill SS, Singh H, Kumar R, Kumar V (2022) Recycling of Ti6Al4V machining swarf into additive manufacturing feedstock powder to realise sustainable recycling goals. J Clean Prod 348:131342
11. Razumov NG, Masaylo DV, Silin AO, Borisov EV, Ozerskoy NE, Goncharov IS, Popovich AA (2021) Investigation of additive manufacturing from the heat-resistant steel powder produced by recycling of the machining chips. J Manuf Process 64:1070–1076
12. Murray JW, Speidel A, Jackson-Crisp A, Smith PH, Constantin H, Clare AT (2021) Unprocessed machining chips as a practical feedstock in directed energy deposition. Int J Mach Tools Manuf 169:103803
13. Dhami HS, Panda PR, Viswanathan K (2022) Production of powders for metal additive manufacturing applications using surface grinding. Manufacturing Letters 32:54–58
14. Jackson MA, Morrow JD, Thoma DJ, Pfefferkorn FE (2020) A comparison of 316 L stainless steel parts manufactured by directed energy deposition using gas-atomized and mechanically-generated feedstock. CIRP Ann Manuf Technol 69:165–168
15. Wolff S, Haddad M, Zhang J, Luo A (2024) Effect of recycled swarf and spherical Ti-6Al-4V feedstocks on laser directed energy deposition additive manufacturing. CIRP Ann Manuf Technol 73:193–196
16. Rojas-Díaz LM, Verano-Jiménez LE, Muñoz-García E, Esguerra-Arce J, Esguerra-Arce A (2020) Production and characterization of aluminum powder derived from mechanical saw chips

and its processing through powder metallurgy. Powder Technol 360:301–311
17. Cherkasova M, Samukov A, Goncharov I, Mezenin A (2020) Influence of the metal chips disintegration method on the physical and mechanical properties of metal powders obtained Vibroengineering Procedia 32:32–37
18. https://www.matweb.com/, accessed on 14/04/2025.
19. Gusev AI, Kurlov AS (2008) Production of nanocrystalline powders by high-energy ball milling: model and experiment. Nanotechnology 19:265302
20. ASTM B213–17, Standard test methods for flow rate of metal powders using the Hall Flowmeter Funnel, ASTM International.
21. Baramate KA, Lacan F, Ryan M, Gangopadhyay S, Bhaduri D (2023) Sustainable manufacturing of metal additive powders from machining scrap, 9th International & 30th All India Manufacturing Technology, Design, and Research Conference (AIMTDR) 2023, IIT BHU, Varanasi, India.
22. Zhou L, Hyer H, Park S, Pan H, Bai Y, Rice KP, Sohn Y (2019) Microstructure and mechanical properties of Zr-modified aluminum alloy 5083 manufactured by laser powder bed fusion. Addit Manuf 28:485–496
23. Mahmood K, Ul Haq Syed W, Pinkerton AJ (2011) Innovative reconsolidation of carbon steel machining swarf by laser metal deposition. Opt Lasers Eng 49:240–247
24. Material Property Data for AISI 1020, AA6082 and AA5083. www.matweb.com. Accessed 06/07/2024
25. Zegzulka J, Gelnar D, Jezerska L, Prokes R, Rozbroj J (2020) Characterization and flowability methods for metal powders. Sci Rep 10:21004
26. Bhaduri D, Ghara T, Penchev P, Paul S, Pruncu CI, Dimov S, Morgan D (2021) Pulsed laser polishing of selective laser melted aluminium alloy parts. Appl Surf Sci 558:149887
27. Rajaseelan SL, Kumarsamy S (2020) Mechanical properties and microstructural characterization of dissimilar friction stir welded AA5083 and AA6061 aluminium alloys. Mechanika 26(6):545–552
28. Bhaduri D, Penchev P, Essa K, Dimov S, Carter LN, Pruncu CI, Pullini D (2019) Evaluation of surface/interface quality, microstructure and mechanical properties of hybrid additive-subtractive aluminium parts. CIRP Ann Manuf Technol 68(1):237–240
29. AlMangour B, Grzesiak D, Yang J-M (2018) In Situ Formation of TiC-Particle-Reinforced stainless steel matrix nanocomposites during ball milling: feedstock powder preparation for selective laser melting at various energy densities. Powder Technol 326:467–478
30. Bhaduri D, Baramate KA, Gangopadhyay S, Davies TE (2025) Circular manufacturing of binder jetting additive parts from Ti-6Al-4V machining chips. CIRP Annals - Manufacturing Technology (in press)

Publisher's Note Springer Nature remains neutral with regard to jurisdictional claims in published maps and institutional affiliations.